ACS Catalysis

Research Article

pubs.acs.org/acscatalysis

Platinum/Gold Alloy Nanoparticles-Supported Hydrotalcite Catalyst for Selective Aerobic Oxidation of Polyols in Base-Free Aqueous Solution at Room Temperature

Duangta Tongsakul, Shun Nishimura, and Kohki Ebitani*

School of Materials Science, Japan Advanced Institute of Science and Technology (JAIST) 1-1 Asahidai, Nomi 923-1292, Japan

Supporting Information

ABSTRACT: As-prepared platinum/gold alloy nanoparticles-supported hydrotalcites (Pt_xAu_y–starch/HTs) by using a soluble starch as a green reducing and a stabilizing agent are found to be truly effective heterogeneous catalysts for the selective aerobic oxidation of glycerol (GLY) and 1,2-propanediol (PG) in base-free aqueous solution using molecular oxygen in atmospheric pressure at room temperature. The Pt_xAu_y–starch/HTs exhibited higher selectivities for oxidation of the primary hydroxyl group in GLY and PG toward glyceric acid (GA) and lactic acid (LA), respectively, with molecular oxygen in aqueous solution than those reactions over monometallic Pt–starch/HT or Au–starch/HT. $Pt_{60}Au_{40}$–starch/HT was found to be the most active catalyst for selective aerobic oxidation of polyols. It showed 73% GLY conversion with 57% GA yield and 63% PG conversion with 47% LA yield and retained high selectivity in recycling experiments. XRD patterns of the Pt_xAu_y–starch NPs indicated the d-spacing of Pt atoms was changed by alloying with Au atoms. XPS and XANES analyses suggested that Pt atoms gained more electrons than Au atoms in Pt_xAu_y–starch/HTs as a result of the two types of electron transfers: (1) from the starch ligand to both Au and Pt atoms and (2) from Au to Pt atoms. We concluded that the high activity and selectivity of Pt_xAu_y–starch/HT can be explained in terms of alterations of geometric and electronic states of the catalytically active surface Pt sites by Au atoms and starch ligand.

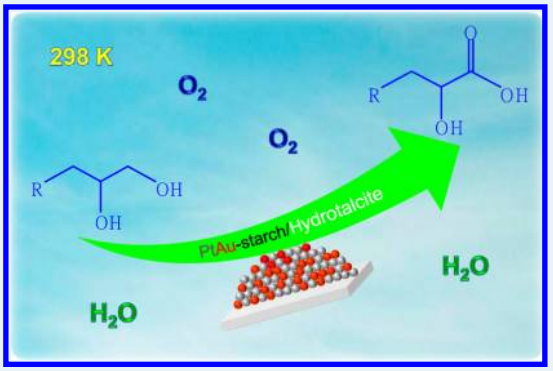

KEYWORDS: *base-free polyol oxidation, heterogeneous catalyst, hydrotalcite, platinum/gold alloy, electronic effect, geometric effect, starch ligand*

1. INTRODUCTION

Biomass is biological material derived from plants, and the transformation of biomass-derived compounds into energy sources and valuable chemicals will serve as an alternative resource instead of fossil fuel.[1−3] Biodiesel fuel (BDF) is the one of biomass-derived energy produced by transesterification of biomass (triglycerides) with alcohols, and a huge amount of glycerol (GLY) is obtained as a byproduct during the production of BDF.[4−6] GLY-derived products can serve various substrates for the manufacture of high-end chemicals. For instance, from the controlled partial oxidation of GLY, various value-added chemicals, such as glyceric acid (GA), dihydroxyacetone, and tartronic acid (TA), can be provided.[4,5,7] Particularly, GA is a very important one, affording medicine and skin care treatment.[1,7−9] In addition, 1,2-propanediol (PG), the product of GLY hydrogenolysis,[10] is a crucial starting material for the chemical synthesis of lactic acid (LA) by a partial oxidation.[5,6,11] LA is used in the industrial fields of food and pharmaceutical products.[12,13]

General reaction pathways for the oxidation of GLY and PG are shown in Scheme 1. Research on supported monometallic nanoparticle (NP) catalysts, especially Pt, Au, and Pd catalysts, for the oxidation of polyols in the presence of base have been reported during the past decade.[14−19] Many publications have detailed that the supported bimetallic NPs also possessed a catalytic activity superior to the monometallic ones for oxidation of polyols in the presence of base (Supporting Information Tables S1 and S2).[11,14,20−24] For example, Dimitratose et al. found that alloyed AuPd/TiO_2 improved activity and selectivity for PG oxidation to LA in the presence of NaOH under pressurized oxygen (10 atm) at 333 K.[14] Brett et al. observed that the addition of Pd to Au atoms significantly enhanced the activity and retained high selectivity to methyl lactate in the presence of sodium methoxide (NaOMe) at 373 K under pressurized oxygen (3 atm).[11]

It is well-known that the catalysis for the oxidation reaction of polyols (e.g., GLY) strongly depends on the basicity of the reaction medium because the external base can enhance a proton abstraction step from the hydroxyl group of GLY. However, the salt of the products, such as glycerate, was formed when a homogeneous base was used, and then the obtained products required an additional neutralization or acidification.

Received: June 17, 2013
Revised: August 13, 2013

   dx.doi.org/10.1021/cs400458k | ACS Catal. 2013, 3, 2199−2207

Scheme 1. General Reaction Pathways for the Oxidation of GLY and PG

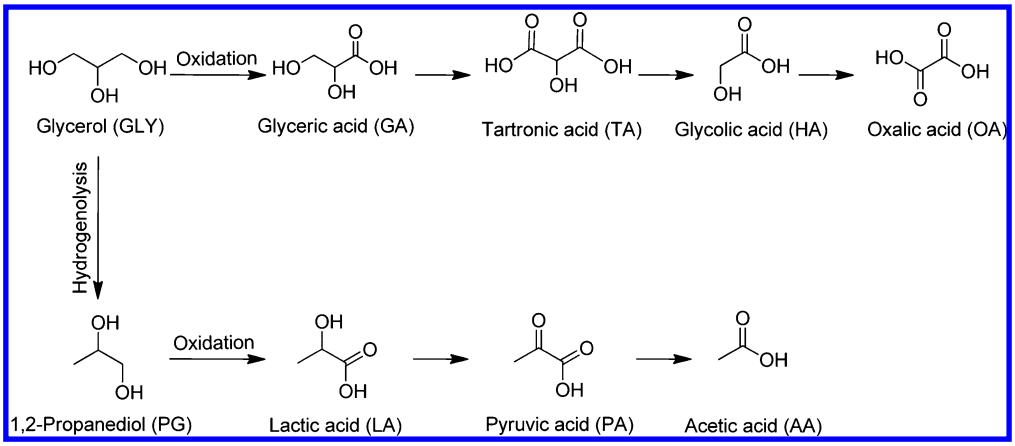

In advanced research, the oxidation reaction has been performed with metal species supported on basic materials, which permitted a base-free oxidation, producing the carboxylic acid rather than the salt form. The modern oxidation process prefers an atmospheric pressure of molecular oxygen (O_2) as a green oxidant because the classical oxidant, such as CrO_3 and $KMnO_4$, had large harmful impacts for the environment.[15,25,26] Recently, the catalytic oxidation of GLY over a bimetallic catalyst in base-free aqueous solution under oxygen flow has been reported. Hou and co-workers showed that PtCu/C and PtSb/multiwall carbon nanotubes (MWCNTs) were more active and selective toward GA than Pt/C and Pt/MWCNT, respectively.[27−29] Tomishige et al. also found that PdAg/C showed higher activity and selectivity to dihydroxyacetone than Pd/C for GLY oxidation with molecular oxygen (3 atm) under neutral conditions at 373 K.[30]

Very recently, we succeeded in the synthesis of a novel hydrotalcite-supported Pt−starch NPs (Pt−starch/HT) catalyst using soluble starch as a green reducing and a stabilizing agent.[31] The Pt−starch/HT became an environmentally friendly and a highly efficient catalyst which suppressed the overoxidation of GLY to C_1 products in comparison with the bare Pt/HT catalyst[32] for selective oxidation of GLY in base-free aqueous solution with molecular oxygen under atmospheric pressure. This achievement inspired us to further challenge for the preparation of an efficient bimetallic NP catalyst in selective oxidation of polyols.

Herein, we explore the efficient catalytic oxidation of polyols (GLY and PG) in base-free aqueous solution under ambient conditions over HT-supported Pt_xAu_y−starch NPs (Pt_xAu_y−starch/HT) catalysts. The Pt_xAu_y−starch/HTs were prepared by a sol immobilization method with various Pt/Au molar ratios (x/y) using soluble starch as a green reducing and stabilizing agent.[31,33] HT is well-known as a reusable basic layered double hydroxide that is frequently used as a support for Pd, Ru, and Au species.[34,35] Following the results shown below, we found that the Pt_xAu_y−starch/HT catalysts exhibited high selectivities for GA and LA formation in aerobic and aqueous base-free oxidations of GLY and PG under ambient conditions (i.e., room temperature and an atmospheric pressure of molecular oxygen). The negative charge on Pt atoms induced by the electron transfer from both neighbor Au atoms and starch ligand were detected by XPS and XANES analyses. We suggested that both geometric and electronic change of the catalytically active Pt sites by adjacent Au atoms and starch ligands contributed to improvement of the activity and selectivity toward the target products.

2. EXPERIMENTAL SECTION

2.1. Chemicals. Hexachloroplatinic acid ($H_2PtCl_6·6H_2O$, 99.9%), tetrachloroauric acid ($HAuCl_4·4H_2O$, 99.9%), 1,2-propanediol (99%), and soluble starch were purchased from Wako Pure Chemicals. Sodium hydroxide (NaOH, 97%) was obtained from Kanto Chemicals. Glycerol (99.9%) was provided by Nacalai Tesque. Hydrotalcite (HT, Mg/Al = 5) was obtained from Tomita Pharmaceutical. 2,6-Di-*tert*-butyl-*p*-cresol (BHT) was received from Tokyo Chemical Industry.

2.2. Preparation of Hydrotalcite Supported Platinum/Gold Catalysts. First, the dispersions of Pt_xAu_y−starch NPs at various metal ratios were synthesized by a chemical reduction method using soluble starch as a reducing and a stabilizing agent. Different ratios of $H_2PtCl_6·6H_2O$ (x mmol) and $HAuCl_4·4H_2O$ (y mmol) were mixed ($x + y = 0.05$ mmol (const.)) with 5 mL of aqueous starch solution (0.2 g starch content) and stirred for 90 min, then the pH of the metal solution was adjusted to neutral with 1 M NaOH. Thereafter, an additional 5 mL of NaOH (0.05 M) was added before heating to 373 K. After refluxing for 20 min, 0.5 g of HT was added to the solution with vigorous stirring, then the mixture was continuously refluxed for 1 h. The theoretical metal loading on HT was 0.1 mmol·g^{-1}. Finally, the solution was cooled to room temperature, filtered, and washed with deionized water. The solid catalyst was dried overnight at 373 K.

2.3. Catalytic Activity for Aerobic Oxidation of Polyols. The catalytic activity of Pt_xAu_y−starch/HT was evaluated for oxidation of polyols (GLY and PG) under a base-free aqueous solution at room temperature with an atmospheric pressure of oxygen. All reactions were performed in a 30 mL Schlenk tube attached to a reflux condenser. The general reaction procedures were as follows: GLY or PG (0.5 mmol), H_2O (2 mL), catalyst (20 mg), temperature (298 K), stirring rate (500 rpm). After the reaction, the catalyst was separated by filtration. The filtrate was analyzed by a high performance liquid chromatography (HPLC) apparatus equipped with an Aminex HPX-87H column (Bio-Rad Laboratories) and a refractive index (RI) detector. The analysis conditions were set as follows: eluent, aqueous solution of H_2SO_4 (10 mM); flow rate, 0.5 mL·min^{-1}; column temperature, 323 K. Turnover frequency (TOF) was calculated by the slope in the initial rate period (0−30 min) of the production of

dx.doi.org/10.1021/cs400458k | ACS Catal. 2013, 3, 2199−2207

Table 1. Results of GLY Oxidation over Pt_xAu_Y–starch NPs/HT Catalysts[a]

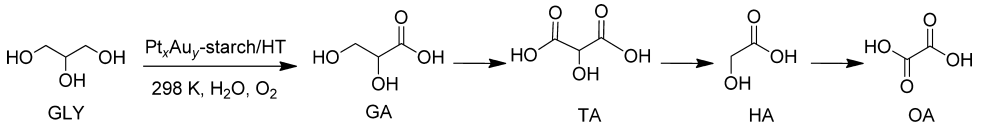

entry	catalysts	conv. of GLY/%	sel. of GA/%	yield/% GA	TA	HA	OA	total metal loading/mmol·g^{-1}c[c]	particle size/nm	TOF (h^{-1})
1	Pt_{100}–starch/HT	88	48	42	13	11	12	0.087	2.0	70.4
2	$Pt_{80}Au_{20}$–starch/HT	80	64	51	10	8	7	0.086	2.2	81.1
3	$Pt_{60}Au_{40}$–starch/HT	73	78	57	9	6	6	0.087	2.2	84.7
4	$Pt_{40}Au_{60}$–starch/HT	74	73	54	10	4	5	0.086	3.8	69.2
5	$Pt_{20}Au_{80}$–starch/HT	50	84	42	4	2	1	0.089	5.4	34.8
6	Au_{100}–starch/HT	trace, 11[b]	–, 37[b]	trace, 4[b]	0, 3[b]	0, 3[b]	0, 1[b]	0.087	5.5	
7	Au/HT	trace		trace	0	0	0	0.096	3.2	

[a]Reaction conditions: GLY, 0.5 mmol; H_2O, 2 mL; catalyst, 20 mg; GLY/metal = 287; oxygen flow, 10 mL·min^{-1}; room temperature, 298 K; reaction time, 6 h. [b]333 K. [c]Analysis by ICP–AES.

main product (GA or LA) per mol of total metal loading on the Pt_xAu_y–starch/HT catalyst in the reaction mixtures.[36]

2.4. Characterization. The morphology of Pt_xAu_y–starch/HT was observed by transmission electron microscopy (TEM; Hitachi H-7100) at 100 kV accelerating voltage. The Pt_xAu_y–starch/HT was dispersed in deionized water and dropped onto a copper grid, then dried overnight in a desiccator. Powder X-ray diffraction (XRD) patterns were obtained with a Rigaku Smartlab X-ray diffractometer using Cu Kα radiation (λ = 0.154 nm) at 40 kV and 20 mA. Inductively coupled plasma atomic emission spectroscopy (ICP–AES) was performed on a Shimadzu ICPS-7000, version 2, to estimate the real concentration of Pt and Au on the catalyst. Ultraviolet and visible (UV–vis) spectra were measured using a Perkin-Elmer Lambda35 spectrometer at room temperature with a light path length of 1 cm. X-ray photoelectron spectroscopy (XPS) was measured on a Shimadzu Kratos AXIS-ULTRA DLD spectrometer using Al target at 15 kV and 10 mA. The binding energies were calibrated with the C 1s peak (284.5 eV) as the internal standard reference. X-ray absorption near-edge structure (XANES) in the Pt L_3-edge and Au L_3-edge were recorded at beamline BL01B1 of SPring-8 with the approval of the Japan Synchrotron Radiation Research Institute (JASRI) (Proposals Nos. 2011A1607 and 2012B1610). The Pt_xAu_y–starch/HT catalysts were grained and pressed to a pellet ($\phi \sim$ 10 mm) for XANES analysis. The obtained XANES spectra were analyzed using the Athena software (version 0.8.056).

3. RESULTS AND DISCUSSION

3.1. Aerobic Oxidation of Glycerol. Results of activity over Pt_xAu_y–starch/HT catalysts for the aerobic GLY oxidation under atmospheric conditions are summarized in Table 1, together with total metal loading and mean particle size. All catalysts except for Au_{100}–starch/HT promoted the selective oxidation toward GA, and minor amounts of tartronic acid (TA), glycolic acid (HA), and oxalic acid (OA) were also observed. The formation of dihydroxyacetone, oxidation at the secondary hydroxyl group, was not detected in all cases. It was consistent with previous reports that GA was obtained as the major product, and it could be further oxidized to TA, HA, and OA in the aerobic oxidation of GLY catalyzed by the Pt-based heterogeneous catalyst.[31,32,37−39] The highest GLY conversion (88%) was achieved by Pt_{100}–starch/HT, although it exhibited a low selectivity toward GA (48%) (Table 1, entry 1).

Because the sum of GA, TA, HA, and OA was ~78% yield (89% selectivity), another overoxidation product toward C_1 product (ex. CO_2) seemed to be expected in Pt_{100}–starch/HT. As the Au amounts increased from y = 20 to 80, the GLY conversion gradually decreased with increasing selectivity for GA and suppressed overoxidation to the formation of byproduct (Table 1, entries 2–5), when the sum of product selectivity is nearly 100%. Au_{100}–starch/HT was inactive at room temperature (RT), whereas it showed a small activity at 333 K (Table 1, entry 6), even though its exhibited particle size of 5.5 nm was similar to that of $Pt_{20}Au_{80}$–starch/HT (5.4 nm). The aerobic oxidation over bare Au/HT with 3.2 nm was also inactive at RT (Table 1, entry 7). Thus, the aerobic oxidation over a supported Au catalyst cannot proceed at RT. These results suggest that the replacement of active Pt atoms with inactive Au atoms likely has some roles for prohibition of overoxidation, and it supports increasing the mass balance close to 100%. The $Pt_{60}Au_{40}$–starch/HT showed the most effective catalyst with a TOF of 84.7 h^{-1} at RT (Table 1, entry 3).

The time profile of the GLY oxidation over $Pt_{60}Au_{40}$–starch/HT is plotted in Figure 1. The reaction was accomplished by

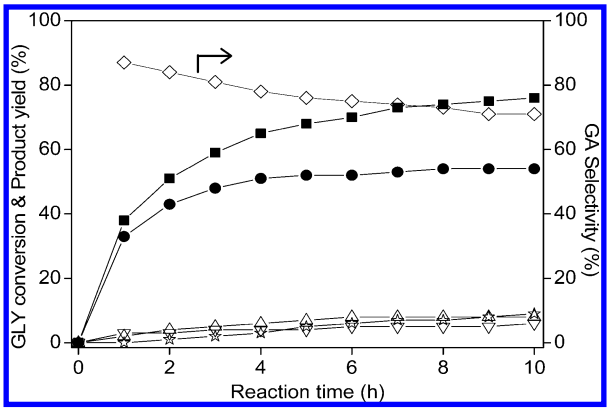

Figure 1. Time course of GLY oxidation catalyzed by $Pt_{60}Au_{40}$–starch/HT: GLY conversion (■), GA yield (●), TA yield (Δ), HA yield (▽), OA yield (☆), and GA selectivity (◊). Reaction conditions: GLY, 0.5 mmol; H_2O, 2 mL; catalyst, 20 mg; oxygen flow, 10 mL·min^{-1}; room temperature (298 K).

dx.doi.org/10.1021/cs400458k | ACS Catal. 2013, 3, 2199−2207

Table 2. Results of PG Oxidation over Pt_xAu_Y–Starch/HT Catalysts[a]

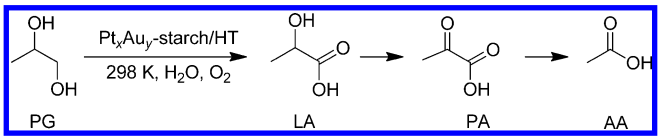

entry	catalysts	conv. of PG/%	sel. of LA/%	yield/% LA	PA	AA	total metal loading/mmol·g^{-1} [c]	particle size/nm	TOF (h^{-1})
1	Pt_{100}–starch/HT	23	82	19	2	2	0.087	2.0	45.1
2	$Pt_{80}Au_{20}$–starch/HT	38	75	28	6	3	0.086	2.2	61.8
3	$Pt_{60}Au_{40}$–starch/HT	39, 63[b]	74, 75[b]	29, 47[b]	6, 12[b]	1, 3[b]	0.087	2.2	62.3,77.2[b]
4	$Pt_{40}Au_{60}$–starch/HT	38	74	28	7	1	0.086	3.8	43.6
5	$Pt_{20}Au_{80}$–starch/HT	27	75	20	4	1	0.089	5.4	21.6
6	Au_{100}–starch/HT	trace		trace	0	0	0.087	5.5	

[a]Reaction conditions: PG, 0.5 mmol; H_2O, 2 mL; catalyst, 20 mg, (PG/metal = 287; PG/metal = 179); oxygen flow, 10 mL·min^{-1}; room temperature, 298 K; reaction time, 6 h. [b]Catalyst, 20 mg; PG/metal = 32 mg; reaction time, 16 h. [c]Analysis by ICP–AES.

the oxidation of the primary hydroxyl group of GLY to GA, together with the formation of side products (i.e., TA, HA and OA) via the overoxidation. At the initial stage of the reaction within 1 h, the highest selectivity to GA (87%) was achieved. Nevertheless, the glyceraldehyde, which was expected to be an intermediate, was not observed. The GLY conversion and yield of GA are 68% and 52%, respectively, as the reaction time reaches 5 h. When the reaction time was increased to 10 h, nearly 80% conversion of GLY was obtained. There was no significant increase in the GA yield after a reaction time of 5 h. A small amount of the overoxidation of GA to TA and further C–C bond cleavage to HA and OA scarcely occurred during the reaction. Although the pH values were gradually decreased with the progressive reaction that we reported on previously,[31] the basicity of the HT support seems to be enough for further reaction because the PtAu/HT catalyst was recyclable for 3 runs (vide infra). Previous reports on GLY oxidation at near room temperature are summarized in Supporting Information Table S1.[21,22,40–42] Most reactions were carried out in the presence of NaOH under pressurized oxygen (3–10 atm). The oxidation of GLY under pressurized oxygen (3 atm) with GLY conversions of 30% and 43% over AuPd (1:3)/MgO and AuPt (1:3)/MgO has also been reported.[37]

3.2. Aerobic Oxidation of 1,2-Propanediol. To confirm the highly selective catalysis at the primary hydroxyl group of C_3 polyol under ambient conditions, Pt_xAu_y–starch/HT catalysts were further applied for the aerobic oxidation of PG. The selective oxidation at the primary hydroxyl group of PG to LA as a main product was observed over Pt_xAu_y–starch/HT except for Au_{100}–starch/HT (Table 2). LA was also previously obtained as the main product in the PG oxidation reaction.[14,15] PG conversion of 23% was found over Pt_{100}–starch/HT (Table 2, entry 1), and it was further enhanced as the Au content was increased, y = 20–60 (Table 2, entries 2–4). Thereafter, the conversion dropped to 27% and trace amounts at y = 80 and 100, respectively (Table 2, entries 5 and 6). The $Pt_{60}Au_{40}$–starch/HT also showed the most effective catalysis for PG oxidation with TOF of 62.3 h^{-1} at RT (Table 1, entry 3).

Figure 2 shows the time profile of PG oxidation over the $Pt_{60}Au_{40}$–starch/HT. Lactaldehyde, which was expected to be an intermediate, was not observed. After the reaction was prolonged to 16 h, the high conversion of 63% was achieved with selectivity to LA of 75%. In addition, the overoxidation of LA to pyruvic acid (PA) followed by C–C bond cleavage to acetic acid (AA) did not occur until after 4 h reaction. Previous

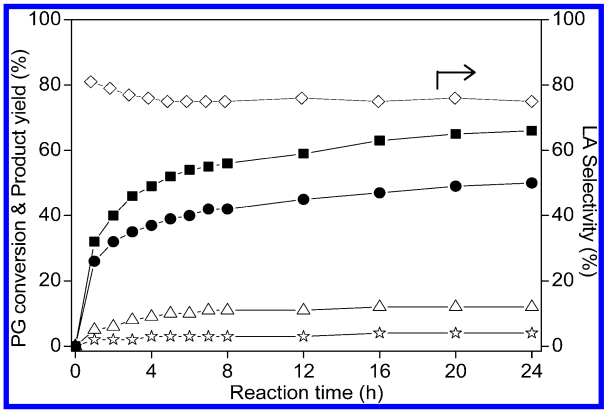

Figure 2. Time course of PG oxidation catalyzed by $Pt_{60}Au_{40}$–starch/HT: PG conversion (■), LA yield (●), PA yield (Δ), AA yield (☆), and LA selectivity (◊). Reaction conditions: PG, 0.5 mmol; H_2O, 2 mL; catalyst amount, 32 mg; oxygen flow, 10 mL·min^{-1}; room temperature (298 K).

reports on PG oxidation are summarized in the Supporting Information, Table S2.[14–19] Most of them required basic conditions and pressurized oxygen.

To examine the stability of the $Pt_{60}Au_{40}$–starch/HT catalyst, the recycling experiments were carried out. After 6 and 16 h of reaction for GLY and PG oxidation, the catalyst was centrifuged, washed with deionized water, and dried under vacuum, then it was employed for further oxidation reaction under the same reaction conditions. Figure 3 indicates that the catalyst slightly decreased in activity but retained high selectivity during the recycling experiment in the oxidations of GLY and PG. The morphology of the recycled catalysts from glycerol oxidation was investigated by TEM. Although the particle size was slightly increased after the reaction (Supporting Information Figure S2), it scarcely influenced its activity for glycerol oxidation.

To evaluate the reaction pathway of aerobic oxidation of polyols over $Pt_{60}Au_{40}$–starch/HT, the reaction was operated in the presence of a radical scavenger (BHT), as shown in Figure 4. BHT slightly influenced the initial oxidation rate of the oxidation of the polyols; however, after prolonged reaction time, the yields of GA and LA in the presence and absence of BHT were the same. This result suggests that the aerobic oxidation over $Pt_{60}Au_{40}$–starch/HT did not proceed through the free-radical mechanism.

dx.doi.org/10.1021/cs400458k | ACS Catal. 2013, 3, 2199–2207

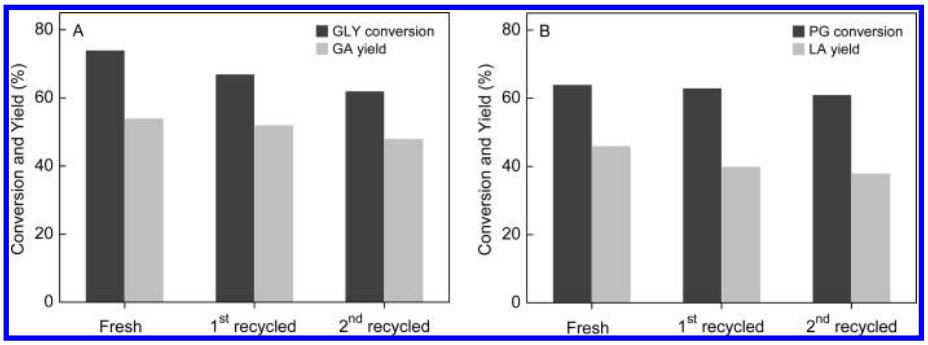

Figure 3. Recycling of $Pt_{60}Au_{40}$–starch/HT catalyst. Reaction conditions: H_2O, 2 mL; oxygen flow, 10 mL·min^{-1}; room temperature (298 K). (A) GLY, 0.5 mmol; catalyst, 20 mg; reaction time, 6 h. (B) PG, 0.5 mmol; catalyst, 32 mg; reaction time, 16 h.

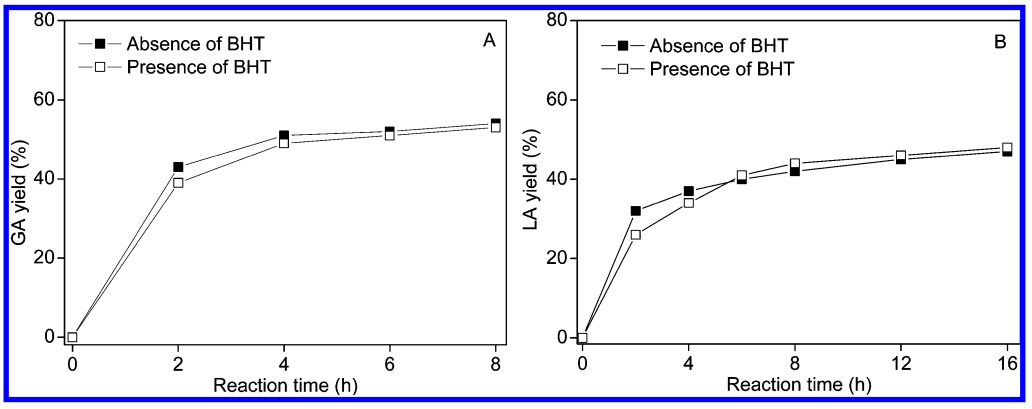

Figure 4. Time course of aerobic oxidation of (A) GLY and (B) PG over $Pt_{60}Au_{40}$–starch/HT catalyst in the absence (■) or presence (□) of BHT. Reaction conditions: H_2O, 2 mL; oxygen flow, 10 mL·min^{-1}; room temperature (298 K). (A) GLY, 0.5 mmol; catalyst, 20 mg. (B) PG, 0.5 mmol; catalyst, 32 mg. BHT/polyol = 1/10 (11 mg).

3.3. Characterization of Pt_xAu_y–starch/HT Catalysts.

First, the morphology of the Pt_xAu_y–starch/HT catalysts was analyzed by TEM. TEM images and mean particle size distribution histograms for all catalysts are shown in Figure 5. Bimetallic NPs were well-dispersed on the surface of HT and showed a narrow size distribution. The particle size of Pt_xAu_y–starch/HTs was near constant with the mean sizes being 2.0, 2.2, and 2.2 nm for y = 0, 20, and 40, respectively. However, increasing the amounts of Au resulted in increasing mean particle sizes, to 3.8, 5.4, and 5.5 nm for y = 60, 80, and 100, respectively (listed in Table 1). Supporting Information Figure S1 shows the UV–vis absorption spectra of Pt_xAu_y–starch NPs. The absorption band (localized surface plasmon resonance) of Au–starch NPs appears around 500–600 nm.[43,44] This characteristic peak of Au–starch NPs was not observed in all Pt_xAu_y–starch NPs spectra, indicating PtAu alloy formation rather than phase-segregated bimetallic NPs.

Figure 6A exhibits the XRD patterns of Pt_xAu_y–starch NPs. All XRD patterns of Pt_xAu_y–starch NPs describe the characteristic of the face-centered cubic (fcc) structure of metallic Pt or Au, the reflection corresponding to the planes (111), (200), (220), (311), and (222).[45] Furthermore, these five diffraction peaks shifted to higher angle with a decrease in the Au amount in each position. For example, the (111) reflection of Pt_xAu_y–starch NPs gradually shifted from 2θ = 38.3, 38.5, 38.8, 39.1, 39.4, and 39.7 with changes in y = 100 to 0. According to the previous literature,[46] 2θ = 38.3 and 39.7 correspond to the (111) reflection of metallic Au and Pt, respectively. Lattice parameters of Pt_xAu_y–starch NPs estimated from the XRD diffraction pattern of (111)[47] as a function of the Au amount are plotted in Figure 6B. The lattice parameters of metallic Pt and Au were 3.92 and 4.07, respectively. Increasing the concentration of Au (y) in Pt_xAu_y–starch NPs leads to an increase in the lattice distance from 3.92 to 3.96, 4.0, 4.03, 4.04, and 4.07 Å, and a linear relationship between the lattice parameter and their composition was obtained. These results indicate that the nanostructures of Pt_xAu_y–starch NPs are homogeneous PtAu alloys.[45]

XPS spectra of Pt_xAu_y–starch NPs are shown in Figure 7. Peaks at 85.6 and 82 eV in Figure 7A were assigned to Au $4f_{5/2}$ and Au $4f_{7/2}$, respectively. All spectra showed the large negative shift to lower binding energy (BE), as compared with Au foil (Au $4f_{5/2}$:88 eV and Au $4f_{7/2}$:84 eV). The same negative shifts also appeared in all peaks around 72 and 68.7 eV attributed to Pt $4f_{5/2}$ and Pt $4f_{7/2}$, respectively, as compared with Pt foil (Pt $4f_{5/2}$:74.4 eV and Pt $4f_{7/2}$:71.2 eV) in Figure 7B. These large negative shifts in both Au 4f and Pt 4f in alloy Pt_xAu_y–starch NPs suggests that a negative charge is loaded on PtAu–starch NPs,[48] which is supposed by the interaction between PtAu–starch NPs and starch ligand. It has been reported that the electron donated from the stabilizer (for example, poly(vinyl pyrrolidone) (PVP)) to a metal such as Pt, Au, and Ag NPs, results in a negative shift of the BE in XPS spectra.[43,49,50] In addition, hydroxyl groups in soluble starch can facilitate the complexation of metal ions to a molecular matrix.[51,52] Therefore, it is supposed that the large negative shift in both Pt 4f and Au 4f are due to electron donation from the starch ligand to both Pt and Au atoms.[53] Considering the peak of Au 4f the decrease in the Au content from y = 100 to 20 leads to a more negative shift in Figure 7A, it was supposedly attributed

dx.doi.org/10.1021/cs400458k | ACS Catal. 2013, 3, 2199–2207

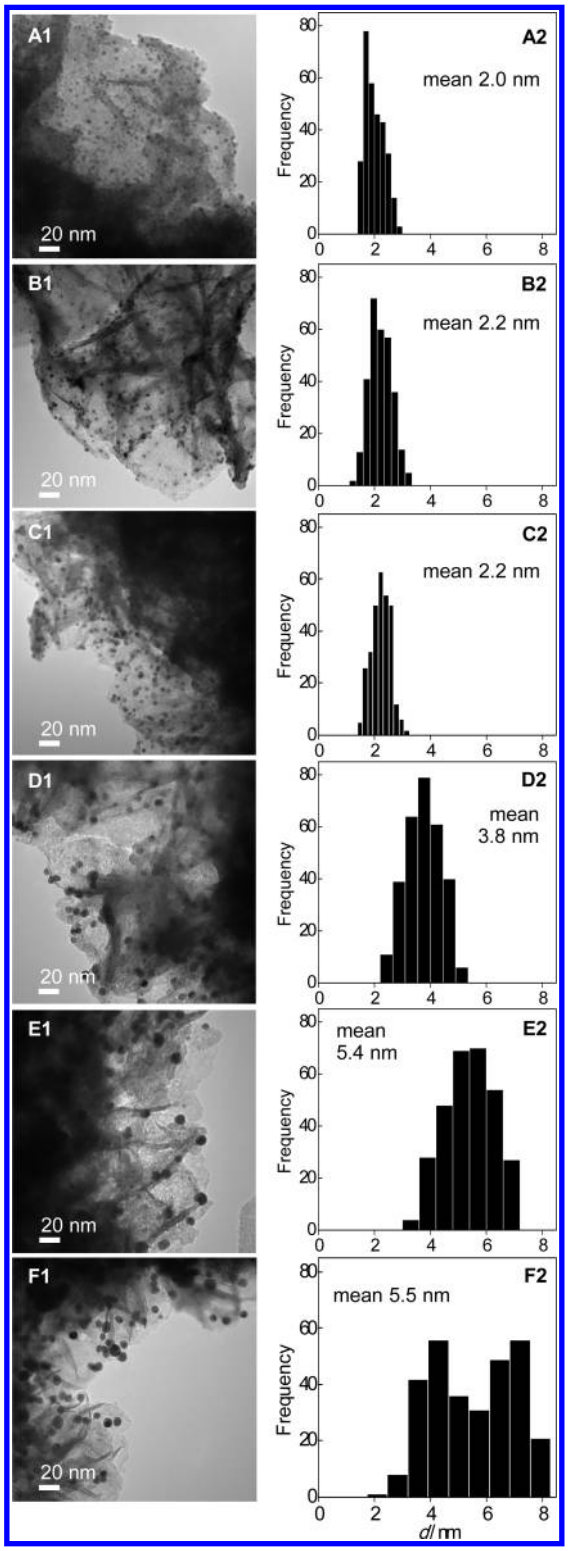

Figure 5. TEM images of Pt_xAu_y–starch/HT: (A1) Pt_{100}–starch/HT, (B1) $Pt_{80}Au_{20}$–starch/HT, (C1) $Pt_{60}Au_{40}$–starch/HT, (D1) $Pt_{40}Au_{60}$–starch/HT, (E1) $Pt_{20}Au_{80}$–starch/HT, and (F1) Au_{100}–starch/HT. (A2–F2) Their particle size distribution histograms.

to decreasing the particle size because the number of ligand-capped surface sites will become larger with the reduced particle size. Although the same phenomenon is also expected to be encountered for Pt 4f, the enhancement of a negative shift of Pt 4f was not observed; even their particle sizes were diminished with a decreasing Au content (Figure 7B). On the contrary, reductions in the negative shift in Pt 4f were found as the Au content was reduced from y = 80 to 0. In other words, the Pt 4f peaks gradually shifted to the lower side of the binding energy. It is postulated that the excess electrons on Au atoms transferred to the adjacent Pt atoms.

Figure 8 shows normalized Pt L_3-edge and Au L_3-edge XANES spectra of Pt_xAu_y–starch/HT. The white-line (WL) feature in the L_3-edge XANES was related to the electron transfer phenomena induced by an X-ray absorption from the p to d states in the element; thus, it indicated the unoccupied densities of the d states.[54,55] Au L_3-edge XANES spectra have no WL feature, since the 5d orbitals full in theory; however, the s–p–d hybridization leads to electron transformation from 5d to the s–p state, leading the small WL intensity in the Au L_3-edge XANES.[55−57] Lower WL intensities than Au foil were oberved for all Au L_3-edges, implicating a Au gained electron (Figure 8B). Figure 9 shows plots of WL intensities in Pt and Au L_3-edges XANES as a function of Au content. The heights of the WL in the Pt L_3-edges gradually became lower, whereas that in Au L_3-edges were higher with an increase of in the Au content. The decreasing tendency of the Pt L_3-edge WL intensity is related to the increase in that of the Au L_3-edge as the Au content increases from y = 20 to 80. Previous works have reported that the NPs' size affected the WL intensity of the XANES spectra. Small NPs reduced the number of metal–metal bonds by the s–p–d hybridization change, resulting in a decrease in the number of d-holes density, leading to a decrease in the WL intensity.[58] As the above result, an increase in the Au content, the size of the Pt_xAu_y–starch NPs increased while the WL intensity of the Pt L_3-edge decreased. Therefore, XPS together with XANES confirmed that a negative charge was present on both the Au and Pt atoms, in which the starch ligand donates electrons, and the excess electrons on the Au atoms can also transfer to the Pt atoms. There have been reports of the electron transfer from Au (EN = 2.54) to Pt (EN = 2.28) in the core–shell structure of NPs, leading to an increase in the active oxygen species on the surface.[59,60] In addition, it has also been reported that a stabilizing/capping agent can play a direct role in regulating the electronic structures.[49,57,61,62] Soluble starch is a linear polymer formed by the α-(1 → 4) linkages between D-glucose units and adopts a left-handed helical conformation in aqueous solution;[52] therefore, it is supposedly possible that the electrons can be transfer via complexation of the starch ligand onto Pt and Au atoms, as illustrated in Scheme 2.

3.4. Oxidation Mechanism. As mentioned, the geometric (d-spacing) and electronic changes of the catalytically active Pt sites by adjacent Au atoms and the starch ligand can lead to improvement of the activity and selectivity to target products. The replacing of active atoms (Pt site) with inactive atoms (Au site) changed the geometry of the Pt surface or modified the strength of the surface adsorption then controlling oxygen coverage.[63−66] $Pt_{60}Au_{40}$–starch/HT showed the highest yield, with a high selectivity for catalytic oxidation of GLY and PG toward GA and LA, respectively, under an atmospheric pressure of molecular oxygen because of both geometric and electronic changes. The reaction mechanism of oxidation of polyols is proposed in Scheme 3. First, O_2 is adsorbed onto the surface of negatively charged Pt atoms (1). It has been reported that anionic metal can activate molecular oxygen by donating an excess electron charge to the antibonding orbital, resulting in the generation of anionic O_2 such as superoxo or peroxo

dx.doi.org/10.1021/cs400458k | ACS Catal. 2013, 3, 2199−2207

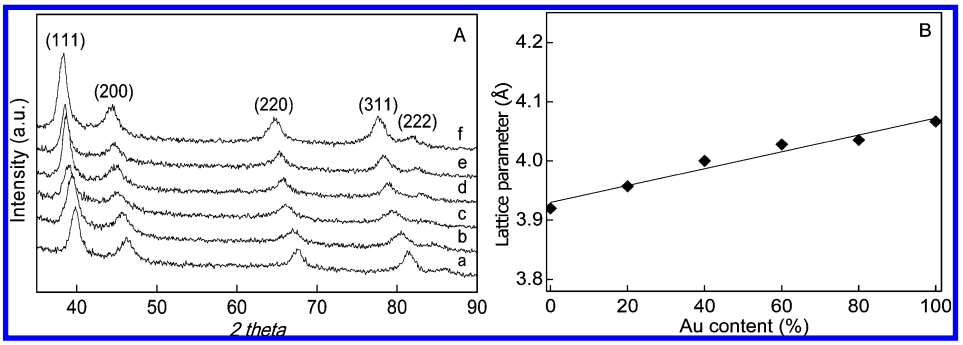

Figure 6. (A) XRD patterns of (a) Au_{100}–starch NPs, (b) $Pt_{20}Au_{80}$–starch NPs, (c) $Pt_{40}Au_{60}$–starch NPs, (d) $Pt_{60}Au_{40}$–starch NPs, (e) $Pt_{80}Au_{20}$–starch NPs, and (f) Pt_{100}–starch NPs. (B) Dependence of the lattice parameters for Pt_xAu_y–starch NPs on the relative composition of the Au amount.

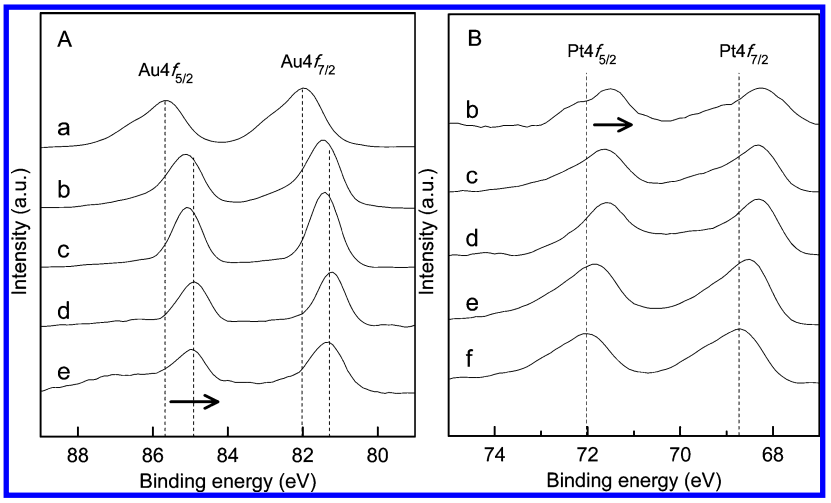

Figure 7. XPS spectra of (A) Au4f and (B) Pt4f of Pt_xAu_y–starch NPs: (a) Au_{100}–starch NPs, 5.5 nm; (b) $Pt_{20}Au_{80}$–starch NPs, 5.4 nm; (c) $Pt_{40}Au_{60}$–starch NPs, 3.8 nm; (d) $Pt_{60}Au_{40}$–starch NPs, 2.2 nm; (e) $Pt_{80}Au_{20}$–starch NPs, 2.2 nm; and (f) Pt_{100}–starch NPs, 2.0 nm.

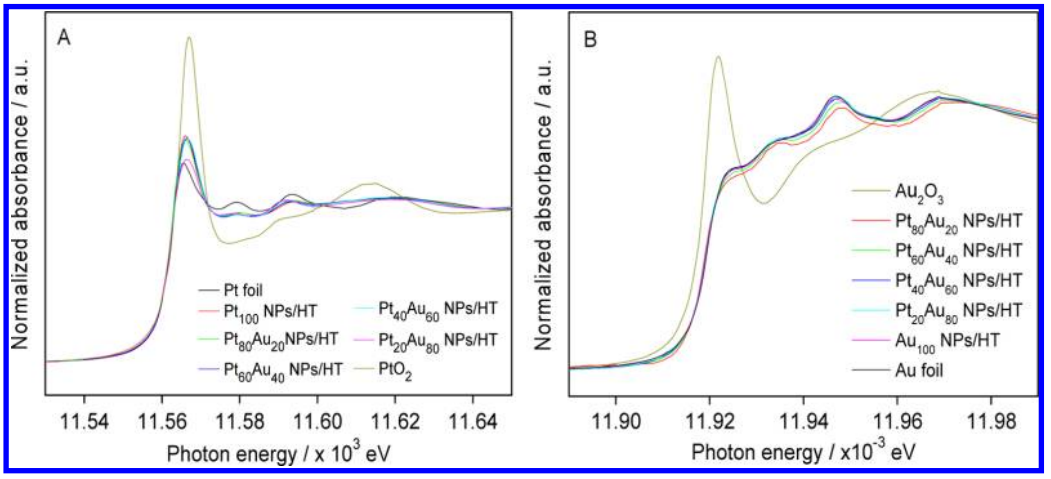

Figure 8. Normalized (A) Pt L_3-edge and (B) Au L_3-edge XANES spectra of Pt_xAu_y–Starch/HT.

oxygen.[67−70] Then the basic support abstracts a proton from the polyol to form the alkoxide, which enhances the polyol's binding to the metal atom (2). The proton in the adsorbed alkoxide carbon is transferred to the adsorbed oxygen; releasing aldehyde (3) and H_2O to generate back the peroxo form (4). Aldehyde, thus formed, is attracted by the adjacent metal atom with adsorbed oxygen (Au atoms) (5). This creates a partial positive charge on the carbonyl carbon. The nucleophilic oxygen atom of water attacks the electron-deficient carbonyl carbon (6). The adsorbed oxygen abstracts the proton to yield carboxylic acid (7) and is changed back to the peroxo form (8) to complete the catalytic cycle.

4. CONCLUSIONS

We explored the efficient and recyclable heterogeneous Pt_xAu_y–starch/HT catalyst for the oxidation of polyols without additional bases under an atmospheric pressure of molecular oxygen. Bimetallic Pt_xAu_y–starch/HT showed higher selectivity

dx.doi.org/10.1021/cs400458k | ACS Catal. 2013, 3, 2199−2207

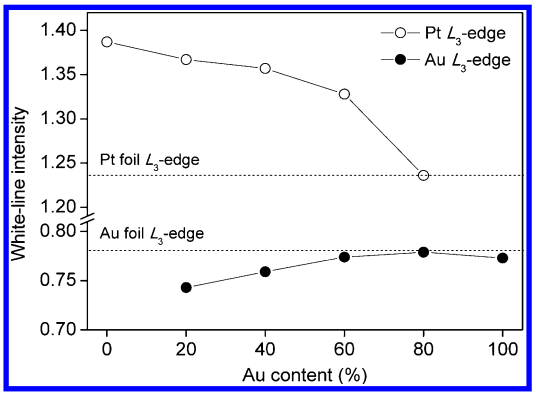

Figure 9. White line intensity of Pt L_3-edge (at 11.565 keV) and Au L_3-edge (at 11.924 keV) XANES spectra of Pt_xAu_y–starch/HT. Dashed lines represent the white-line intensity of Pt and Au foils.

Scheme 2. The Possible Electron Transfer from Starch Ligand to AlloyPtAu–Starch NPs and from Au Atoms to Adjacent Pt Atoms

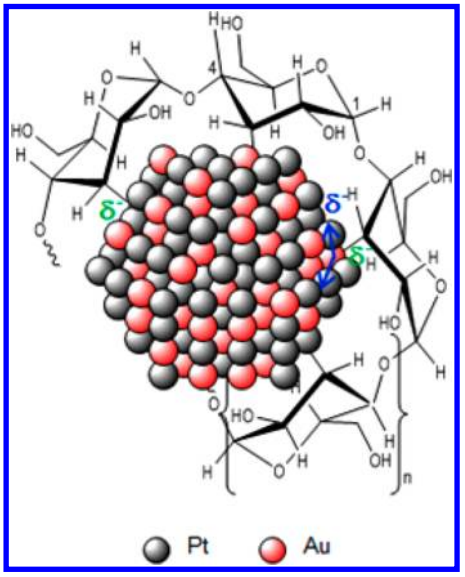

for the oxidation at the primary hydroxyl groups of GLY and PG toward GA and LA, respectively, than those of each monometallic ones. $Pt_{60}Au_{40}$–starch/HT is found to be the most selective catalyst for oxidation of polyols. UV–vis and XRD revealed that Pt_xAu_y–starch formed as an alloy, and their d-spacing was changed from individual metals. XPS and XANES showed the negative charge on both Au and Pt atoms. It was supposed that the PtAu–starch NPs gained charge from the starch ligand. Au L_3-edge XANES spectra revealed an increase in the white-line intensity as the amount of Au was increased, indicating the excess electrons on the Au atoms also transfer to the Pt atoms. The negatively charged Pt atoms may enhance the oxygen absorption and generate anionic O_2 such as superoxo or peroxo oxygen to oxidize polyols. We conclude that the geometric and electronic changes of the catalytically active Pt sites by adjacent Au atoms and the starch ligand lead to improvement of the activity and selectivity to target products.

■ ASSOCIATED CONTENT

Supporting Information

Catalyst performances for GLY and PG oxidation in the previous reports, UV–vis spectra of Pt_xAu_y–starch NPs, and TEM images of recycled $Pt_{60}Au_{40}$–starch/HT catalysts. This information is available free of charge via the Internet at http://pubs.acs.org/.

■ AUTHOR INFORMATION

Corresponding Author

*E-mail: Kohki Ebitani; ebitani@jaist.ac.jp.

Notes

The authors declare no competing financial interest.

■ ACKNOWLEDGMENTS

D.T. gratefully acknowledges support from a grant from the dual Ph.D program between JAIST and Chulalongkorn University. Parts of this research are supported by a Grant-in-Aid for Young Scientists (B) (No. 25820392) and Scientific Research(C) (No. 25420825) promoted by the Ministry of Education, Culture, Sports, Science and Technology (MEXT), Japan. XAFS measurements of the Pt_xAu_y–starch/HTs were performed at the BL01B1 in the SPring-8 by approval of the Japan Synchrotron Radiation Research Institute (JASRI) (Proposals Nos. 2011A1607 and 2012B1610).

■ REFERENCES

(1) Corma, A.; Iborra, S.; Velty, A. *Chem. Rev.* **2007**, *107*, 2411–2502.

Scheme 3. A Proposed Reaction Mechanism for Polyols Oxidation Catalyzed by PtAu–Starch/HT

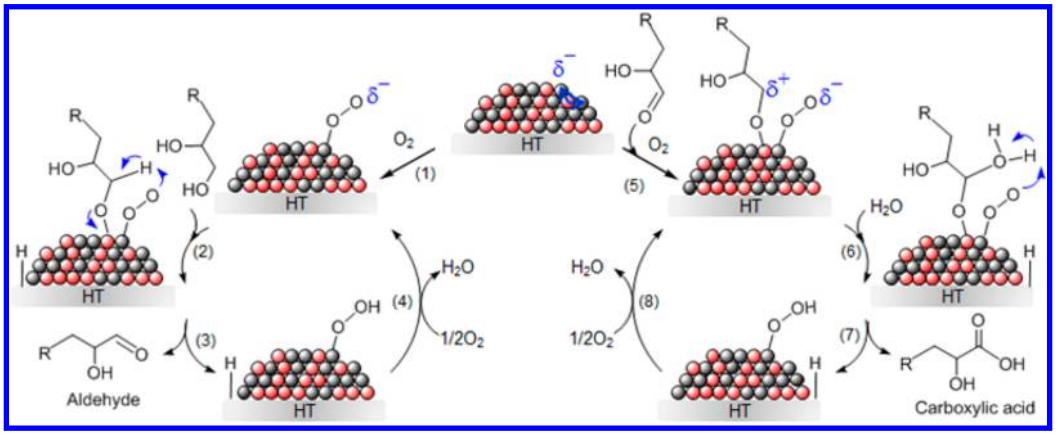

dx.doi.org/10.1021/cs400458k | *ACS Catal.* 2013, 3, 2199–2207

(2) Chheda, J. N.; Huber, G. W.; Dumesic, J. A. *Angew. Chem., Int. Ed.* **2007**, *46*, 7164−7183.
(3) Takagaki, A.; Nishimura, S.; Ebitani, K. *Catal. Surv. Asia* **2012**, *16*, 164−182.
(4) Katryniok, B.; Kimura, H.; Skrzyńska, E.; Girardon, J.-S.; Fongarland, P.; Capron, M.; Ducoulombier, R.; Mimura, N.; Paul, S.; Dumeignil, F. *Green Chem.* **2011**, *13*, 1960−1979.
(5) Zhou, C.-H. (Clayton); Beltramini, J. N.; Fan, Y.-X.; Lu, G. Q. (Max) *Chem. Soc. Rev.* **2008**, *37*, 527−549.
(6) Pagliaro, M.; Ciriminna, R.; Kimura, H.; Rossi, M.; Pina, C. D. *Angew. Chem., Int. Ed.* **2007**, *46*, 4434−4440.
(7) Stockel, R. F. Method of treating dermatological conditions. U.S. Patent 2007/086 977 A1, April 19, 2007.
(8) Gupta, S. K. Novel hydroxyl acid complexes for antiaging and skin renovation. U.S. Patent 2007/092 461 A1, April 26, 2007.
(9) Behr, A.; Eilting, J.; Irawadi, K.; Leschinski, J.; Lindner, F. *Green Chem.* **2008**, *10*, 13−30.
(10) Nakagawa, Y.; Tomishige, K. *Catal. Surv. Asia* **2011**, *15*, 111−116.
(11) Brett, G. L.; Miedziak, P. J.; Dimitratos, N.; Lopez-Sanchez, J. A.; Dummer, N. F.; Tiruvalam, R.; Kiely, C. J.; Knight, D. W.; Taylor, S. H.; Morgan, D. J.; Carley, A. F.; Hutchings, G. J. *Catal. Sci. Technol.* **2012**, *2*, 97−104.
(12) Datta, R.; Henry, M. *J. Chem. Technol. Biotechnol.* **2006**, *81*, 1119−1129.
(13) Lux, S.; Stehring, P.; Siebenhofer, M. *Sep. Sci. Technol.* **2010**, *45*, 1921−1927.
(14) Dimitratos, N.; Lopez-Sanchez, J. A.; Meenakshisundaram, S.; Anthonykutty, J. M.; Brett, G.; Carley, A. F.; Taylor, S. H.; Knight, D. W.; Hutchings, G. J. *Green Chem.* **2009**, *11*, 1209−1216.
(15) Huang, Z.; Li, F.; Chen, B.; Xue, F.; Yuan, Y.; Chen, G.; Yuan, G. *Green Chem.* **2011**, *13*, 3414−3422.
(16) Bianchi, C.; Porta, F.; Prati, L.; Rossi, M. *Top. Catal.* **2000**, *13*, 231−236.
(17) Demirel, S.; Kern, P.; Lucas, M.; Claus, P. *Catal. Today* **2007**, *122*, 292−300.
(18) Taarning, E.; Madsen, A. T.; Marchetti, J. M.; Egeblad, K.; Christensen, C. H. *Green Chem.* **2008**, *10*, 408−414.
(19) Sugiyama, S.; Tanaka, H.; Bando, T.; Nakagawa, K.; Sotowa, K.-I.; Katou, Y.; Mori, T.; Yasukawa, T.; Ninomiya, W. *Catal. Today* **2013**, *230*, 115−120.
(20) Wang, D.; Villa, A.; Porta, F.; Su, D.; Prati, L. *Chem. Commun.* **2006**, 1956−1958.
(21) Bianchi, C. L.; Canton, P.; Dimitratos, N.; Porta, F.; Prati, L. *Catal. Today* **2005**, *102−103*, 203−212.
(22) Dimitratos, N.; Porta, F.; Prati, L. *Appl. Catal., A* **2005**, *291*, 210−214.
(23) Prati, L.; Porta, F.; Wang, D.; Villa, A. *Catal. Sci. Technol.* **2011**, *1*, 1624−1629.
(24) Hu, W.; Knight, D.; Lowry, B.; Varma, A. *Ind. Eng. Chem. Res.* **2010**, *49*, 10876−10882.
(25) Maity, P.; Gopinath, C. S.; Bhaduri, S.; Lahiri, G. K. *Green Chem.* **2009**, *11*, 554−561.
(26) Zhang, H.; Toshima, N. *Catal. Sci. Technol.* **2013**, *3*, 268−278.
(27) Liang, D.; Gao, J.; Wang, J.; Chen, P.; Hou, Z.; Zheng, X. *Catal. Commun.* **2009**, *10*, 1586−1590.
(28) Nie, R.; Liang, D.; Shen, L.; Gao, J.; Chen, P.; Hou, Z. *Appl. Catal., B* **2012**, *127*, 212−220.
(29) Liang, D.; Gao, J.; Wang, J.; Chen, P.; Wei, Y.; Hou, Z. *Catal. Commun.* **2011**, *12*, 1059−1062.
(30) Hirasawa, S.; Nakagawa, Y.; Tomishige, K. *Catal. Sci. Technol.* **2012**, *2*, 1150−1152.
(31) Tongsakul, D.; Nishimura, S.; Thammacharoen, C.; Ekgasit, S.; Ebitani, K. *Ind. Eng. Chem. Res.* **2012**, *51*, 16182−16187.
(32) Tsuji, A.; Rao, K. T. V.; Nishimura, S.; Takagaki, A.; Ebitani, K. *ChemSusChem* **2011**, *4*, 542−548.
(33) Tongsakul, D.; Wongravee, K.; Thammacharoen, C.; Ekgasit, S. *Carbohydr. Res.* **2012**, *357*, 90−97.
(34) Kaneda, K.; Ebitani, K.; Mizugaki, T.; Mori, K. *Bull. Chem. Soc. Jpn.* **2006**, *79*, 981−1016.
(35) Nishimura, S.; Takagaki, A.; Ebitani, K. *Green Chem.* **2013**, *15*, 2026−2042.
(36) Lorenz, H.; Penner, S.; Jochum, W.; Rameshan, C.; Klötzer, B. *Appl. Catal., A* **2009**, *358*, 203−210.
(37) Brett, G. L.; He, Q.; Hammond, C.; Miedziak, P. J.; Dimitratos, N.; Sankar, M.; Herzing, A. A.; Conte, M.; Lopez-Sanchez, J. A.; Kiely, C. J.; Knight, D. W.; Taylor, S. H.; Hutchings, G. J. *Angew. Chem., Int. Ed.* **2011**, *50*, 10136−10139.
(38) Shang, C.; Liu, Z.-P. *J. Am. Chem. Soc.* **2011**, *133*, 9938−9947.
(39) Zope, B. N.; Hibbitts, D. D.; Neurock, M.; Davis, R. J. *Science* **2010**, *330*, 74−78.
(40) Porta, F.; Prati, L. *J. Catal.* **2004**, *224*, 397−403.
(41) Ketchie, W. C.; Murayama, M.; Davis, R. J. *Top. Catal.* **2007**, *44*, 307−317.
(42) Prati, L.; Spontoni, P.; Gaiassi, A. *Top. Catal.* **2009**, *52*, 288−296.
(43) Chen, C.-W.; Akashi, M. *Langmuir* **1997**, *13*, 6465−6472.
(44) Peng, Z.; Yang, H. *Nano. Res.* **2009**, *2*, 406−415.
(45) Antolini, E.; Salgado, J. R. C.; da Silva, R. M.; Gonzalez, E. R. *Mater. Chem. Phys.* **2007**, *101*, 395−403.
(46) Wu, M.-L.; Chen, D.-H.; Huang, T.-C. *Chem. Mater.* **2001**, *13*, 599−606.
(47) Carrettin, S.; McMorn, P.; Johnston, P.; Griffin, K.; Kiely, C. J.; Hutchings, G. J. *Chem. Chem. Phys.* **2003**, *5*, 1329−1336.
(48) Zhang, G.-R.; Xu, B.-Q. *Nanoscale* **2010**, *2*, 2798−2804.
(49) Borodko, Y.; Habas, S. E.; Koebel, M.; Yang, P.; Frei, H.; Somorjai, G. A. *J. Phys. Chem. B* **2006**, *110*, 23052−23059.
(50) Zhang, G.-R.; Xu, B.-Q. *Nanoscale* **2010**, *2*, 2798−2804.
(51) Raveendran, P.; Fu, J.; Wallen, S. L. *J. Am. Chem. Soc.* **2003**, *125*, 13940−13941.
(52) Vigneshwaran, N.; Nachane, R. P.; Balasubramanya, R. H.; Varadarajan, P. V. *Carbohydr. Res.* **2006**, *341*, 2012−2018.
(53) Further study is currently under investigation to clarify this point.
(54) Beck, I. E.; Kriventsov, V. V.; Ivanov, D. P.; Zaikovsky, V. I.; Bukhtiyarov, V. I. *Nucl. Instrum. Methods A* **2009**, *603*, 108−110.
(55) Zhang, P.; Sham, T. K. *Appl. Phys. Lett.* **2002**, *81*, 736−738.
(56) Nishimura, S.; Yakita, Y.; Katayama, M.; Higashimine, K.; Ebitani, K. *Catal. Sci. Technol.* **2013**, *3*, 351−359.
(57) Tsunoyama, H.; Sakurai, H.; Negishi, Y.; Tsukuda, T. *J. Am. Chem. Soc.* **2005**, *127*, 9374−9375.
(58) van Bokhoven, J. A.; Miller, J. T. *J. Phys. Chem. C* **2007**, *111*, 9245−9249.
(59) Zeng, J.; Yang, J.; Lee, J. Y.; Zhou, W. *J. Phys. Chem. B* **2006**, *110*, 24606−24611.
(60) Ortiz-Soto, L. B.; Alexeev, O. S.; Amiridis, M. D. *Langmuir* **2006**, *22*, 3112−3117.
(61) Qiu, L.; Liu, F.; Zhao, L.; Yang, W.; Yao, J. *Langmuir* **2006**, *22*, 4480−4482.
(62) Tsunoyama, H.; Ichikuni, N.; Sakurai, H.; Tsukuda, T. *J. Am. Chem. Soc.* **2009**, *131*, 7086−7093.
(63) Chen, M.; Kumar, D.; Yi, C.-W.; Goodman, D. W. *Science* **2005**, *310*, 291−293.
(64) Rashkeev, S. N.; Lupini, A. R.; Overbury, S. H.; Pennycook, S. J.; Pantelides, S. T. *Phys. Rev. B* **2007**, *76*, 035438-1−035438-8.
(65) Mott, D.; Luo, J.; Njoki, P. N.; Lin, Y.; Wang, L.; Zhong, C.-J. *Catal. Today* **2007**, *122*, 378−385.
(66) Prati, L.; Villa, A.; Campione, C.; Spontoni, P. *Top. Catal.* **2007**, *44*, 319−324.
(67) Chaki, N. K.; Tsunoyama, H.; Negishi, Y.; Sakurai, H.; Tsukuda, T. *J. Phys. Chem. C* **2007**, *111*, 4885−4888.
(68) Okumura, M.; Kitagawa, Y.; Haruta, M.; Yamaguchi, K. *Appl. Catal., A* **2005**, *291*, 37−44.
(69) Gustafsson, K.; Andersson, S. *J. Chem. Phys.* **2004**, *120*, 7750−7754.
(70) Kim, Y. S.; Bostwick, A.; Rotenberg, E.; Ross, P. N.; Hong, S. C.; Mun, B. S. *J. Chem. Phys.* **2010**, *133*, 034501-1−034501-4.